

# Anomaly-aware multiple instance learning for rare anemia disorder classification

Salome Kazemina<sup>1,2</sup>, Ario Sadafi<sup>1,3</sup>, Asya Makhro<sup>4</sup>, Anna Bogdanova<sup>4</sup>, Shadi Albarqouni<sup>5,6,7</sup>, and Carsten Marr<sup>1</sup> (✉)

<sup>1</sup> Institute of AI for Health, Helmholtz Munich – German Research Center for Environmental Health, Neuherberg, Germany

<sup>2</sup> Technical University of Munich, Munich, Germany

<sup>3</sup> Computer Aided Medical Procedures, Technical University of Munich, Munich, Germany

<sup>4</sup> Red Blood Cell Research Group, Institute of Veterinary Physiology, Vetsuisse Faculty and the Zurich Center for Integrative Human Physiology, University of Zurich, Zurich, Switzerland

<sup>5</sup> Clinic for Diagnostic and Interventional Radiology, University Hospital Bonn, Germany

<sup>6</sup> Helmholtz AI, Helmholtz Munich – German Research Center for Environmental Health, Neuherberg, Germany

<sup>7</sup> Faculty of Informatics, Technical University Munich, Munich, Germany

**Abstract.** Deep learning-based classification of rare anemia disorders is challenged by the lack of training data and instance-level annotations. Multiple Instance Learning (MIL) has shown to be an effective solution, yet it suffers from low accuracy and limited explainability. Although the inclusion of attention mechanisms has addressed these issues, their effectiveness highly depends on the amount and diversity of cells in the training samples. Consequently, the poor machine learning performance on rare anemia disorder classification from blood samples remains unresolved. In this paper, we propose an interpretable pooling method for MIL to address these limitations. By benefiting from instance-level information of negative bags (i.e., homogeneous benign cells from healthy individuals), our approach increases the contribution of anomalous instances. We show that our strategy outperforms standard MIL classification algorithms and provides a meaningful explanation behind its decisions. Moreover, it can denote anomalous instances of rare blood diseases that are not seen during the training phase.

**Keywords:** Multiple instance learning · Anomaly pooling · Rare anemia disorder · Red blood cells

## 1 Introduction

The appearance of human red blood cells changes directly with their volume. Typically red blood cells have a discoid concave shape, and as their volume increases or decrease in physiological conditions, they shrivel into star-shaped

cells or swell into spherical shapes [9]. In hereditary hemolytic anemias (HHAs), a cell’s membrane is not formed properly and cannot accommodate volume changes, resulting in the formation of anomalous morphologies. Membrane instability and reduced deformability are other factors in a number of HHAs, such as hereditary spherocytosis, sickle cell disease, and thalassemia, where improper membrane formation leads to irregularly formed cells.

Tools for close monitoring of blood samples in HHA patients is crucial for diagnosis [8], disease progression [4], and severity estimation [17]. However, since most cells in a patient’s sample have no evident morphological feature relevant to the HHA, identifying hallmark cells is a needle-in-the-hay-stack search. Furthermore, presence of a few anomalous cells in a sample does not necessarily link to an underlying condition making the diagnosis even more challenging.

In addition, proper single cell annotation for supervised model training is a cumbersome, expensive task and introduces intra-expert variability. Thus, the automated analysis of blood samples is a perfect problem for multiple instance learning-based approaches. Multiple Instance Learning (MIL) is a weakly supervised learning method, where only bag-level labels are used [3]. Notably, a bag with a negative label does not contain any positive instance, while bags with a positive label may contain negative instances. In other words, the class of a bag depends on the existence of one or more class-related instance. Thus, the learning signal, back-propagated to the instance-level feature extractor may be very weak and ineffective. To address this problem, MIL-based deep classifiers require a large number of training data to perform promisingly [3]. Providing such data is particularly difficult in the case of rare disease. A possible solution is the deployment of intelligent pooling methods to magnify the learning signal back-propagated from informative instances [14]. In basic MIL classifiers, when the bag contains a small number of class-related instances, a typical max or average pooling cannot provide such magnification [14].

Another requirement for health AI applications is explainability. MIL classifiers should thus be able to specify HHA-related structures of instances anomalies. Recently, attention-based pooling mechanisms showed a good performance in tackling both learning signal magnification and explainability challenges [10,14,16]. However, attention mechanisms are prone to fail in scenarios where only a few training samples are available, and consequently, the algorithm can not identify relevant instances in the bags correctly. In HHA classification, such a problem leads to noisy attention scores where lots of disorder-relevant (positive) cells receive low attention, and the distribution of attention on non-disorder (negative) cells would be non-uniform. Here, a strategy accounting for the diversity of disorder-relevant cells and data imbalance is required.

This paper introduces an anomaly-aware pooling method, which is able to address limitations of the attention mechanism with an efficient amount of training data. While instance-level information for positive bags is not available, we exploit negative bag labels that apply to all instances of the bag and estimate the distribution of negative instances using Bayesian Gaussian mixture models. By measuring the distance of instances to this distri-

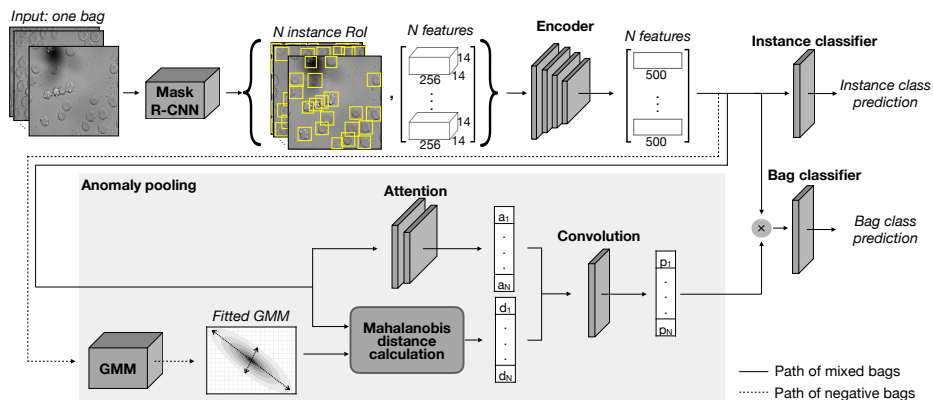


Fig. 1: Overview of our proposed anomaly-aware MIL classifier. A Mask R-CNN outputs detected instance bounding boxes and basic instance features. Then, an encoder maps those features to a latent representation. Dashed path: A GMM distribution is fitted to instances from negative bags  $B_{neg}$ , and its parameters are saved. Solid path: Attention scores  $a_{n \in N}$  and anomaly scores  $d_{n \in N}$  are estimated and combined through a convolution layer to generate pooling weights  $p_{n \in N}$ . Finally, a fully connected layer predicts the bag label.

bution, we define an anomaly score that is used for pooling in addition to learned attention scores. Our method’s performance is explainable by specifying the contribution of instances in the final bag classification. Also, our proposed anomaly score can specify anomalous instances that are rare and haven’t been seen during the training. We make our code publicly available at <https://github.com/marrlab/Anomaly-aware-MIL>.

## 2 Method

Our MIL classifier  $f_\theta$  consists of an instance detector, a deep instance feature extractor  $h_\psi$ , and an attention-anomaly pooling mechanism that assigns a contribution weight to each instance. The input of our classifier is a bag of instances  $\{I_1, \dots, I_N\} \in B$ ; the output is a class  $c_i$  from possible classes defined in  $C$ . In our target application, bags are red blood cells from brightfield microscopic images of blood samples, each containing between 12 to 45 cells (See Fig. 1).

### 2.1 Instance-level feature extraction

**Preprocessing.** Since instance-level information plays a crucial role in bag classification and interpretation, we need to detect them and follow their footprint in the final classification result. For instance detection, we prefer two-stage object detection methods due to the higher accuracy of their performance in comparison with one-stage methods [5]. As a preprocessing step, any two-stage object

detector can be used. We employ Mask R-CNN [6] with ResNet [7] backbone since it provides an accuracy above 91% in detecting instances in microscopic images [5,1]. In our setting, the instance detector takes the bag  $B$  and outputs a bounding box and a feature map for each instance, regardless of their class. We use these feature maps as instances  $I_n \in \{I_1, \dots, I_N\} = B$ . Mask R-CNN extracts features of each instance independently, regardless of its size, scale, and location. This simple step is extremely beneficial in our MIL training as it avoids challenges stemming from non-uniform information distributions of instances, which is widely researched in the literature [12,18,2].

**Instance representation.** Using a 4-layer convolutional encoder  $h_\psi : \mathbb{R}^m \rightarrow \mathbb{R}^k$ , we map each instance  $I_n$  to a point  $z_n$  in the  $k$ -dimensional representation space  $Z$ :

$$z_n = h_\psi(I_n), \quad n \in N \quad (1)$$

## 2.2 Anomaly-aware pooling

**Negative distribution estimation.** We estimate the distribution of negative instances in our latent space and detect anomalies by measuring their distance to this distribution. As a prior assumption, we consider a Gaussian Mixture Model (GMM) probability distribution on negative instance representations. Due to Bayes' rule, the posterior probability distribution would be a GMM as well. Therefore we fit a GMM model  $g_\Gamma$  on negative instance representations. To estimate  $\Gamma$ , we use an Expectation-Maximization (EM) algorithm that maximizes the likelihood  $p(\Gamma|Z_{neg})$  given  $Z_{neg} : \{z_j|I_j \in B_{neg}\}$

$$p(\Gamma|Z_{neg}) = \sum_i \tilde{\gamma}_i \mathcal{N}(\tilde{\mu}_i, \tilde{\Sigma}_i), \quad (2)$$

where  $\tilde{\gamma}_i$ ,  $\tilde{\mu}_i$ , and  $\tilde{\Sigma}_i$  are estimated weight, mean, and covariance matrix of a Gaussian distribution, characterizing the  $i^{th}$  GMM component, respectively. When the algorithm converges, we save the model's parameters as a reference for anomaly scoring.

**Anomaly scoring.** For anomaly scoring we measure the Mahalanobis distance between instances and the  $g_\Gamma$

$$d_n = \sqrt{(z_n - \mu)^T \Sigma^{-1} (z_n - \mu)}, \quad (3)$$

where  $\mu$  and  $\Sigma$  are mean and covariance of the  $g_\Gamma$  distribution. We have chosen Mahalanobis distance over other distances since it considers the distribution's covariance in its distance measurement.

**Attention.** The attention mechanism is a method to extract meaningful instances contributing to the final decision of the model. Specially, in MIL it showed a good performance in both classification and interpretation of deep networks [10,16,13,14,19]. Our deep attention network  $v_\omega$  estimates an attention score  $a_n$  for each instance  $I_n$  as

$$a_n = v_\omega(z_n). \quad (4)$$

**Pooling.** Our pooling mechanism combines attention  $a_n$  and anomaly  $d_n$  scores to estimate a contribution weight for each instance and conclude the latent representation of the bag:

$$z_B = \sum_{n=0}^N (W_{D_n} d_n + W_{A_n} a_{z_n}) z_n. \quad (5)$$

Here  $W_D$  and  $W_A$  are respectively learned parameters, to specify the intervention share of attention and anomaly scores. Finally, a fully connected layer  $f_\theta$  maps the  $k$ -dimensional representation  $z_B$  to a class  $c_i$  (see Fig. 1). Both anomaly and attention scores of an instance are independently calculated and fed to a  $1 \times 1$  convolution to estimate the final pooling weight of the corresponding instance. This makes our pooling method permutation invariant.

### 2.3 Optimization

The functionality of  $v_\omega$  and fitting  $g_\Gamma$  on negative instances highly depends on the encoded instances by  $h_\psi$ . To boost the training procedure, we start with a single instance classifier (SIC)  $s_\zeta$  using noisy labels for learning [16]. In other words, we assign the bag label to all of its instances and calculate a cross-entropy loss ( $\text{CE}_{\text{SIC}}$ ) to optimize the model in the first epochs. Then, by increasing the epoch number  $e$ , we gradually decrease SIC’s impact on the training and conversely increase the MIL cross-entropy loss ( $\text{CE}_{\text{MIL}}$ ) contribution. Therefore, the final loss function, considering a dynamic coefficients  $\beta(e)$ , is defined as:

$$L(\theta, \zeta, \omega, \psi) = (1 - \beta(e))\text{CE}_{\text{MIL}} + \beta(e)\text{CE}_{\text{SIC}}, \quad (6)$$

## 3 Experiment

We applied our classifier on microscopic images of blood samples from HHA patients. In particular, we evaluated three aspects of our method’s functionality: 1) classification, 2) explainability, and 3) rare anomaly recognition.

**Dataset.** Patients previously diagnosed with hereditary spherocytosis, xerocytosis, thalassemia, and sickle cell disease were enrolled in the CoMMiTMenT study. The study protocols were approved by the Medical Ethical Research Board

Table 1: Average classification performance of our proposed method compared to four baselines. The numbers show the mean value along with the standard deviation of metrics measured in 5 runs.

Method	Accuracy	F1-score	AU RoC
Att [10]	0.752±0.009	0.741±0.010	0.826±0.009
Att + SIC [16]	0.770±0.008	0.757±0.009	0.808±0.013
Anomaly	0.630±0.029	0.604±0.026	0.648±0.025
Anomaly + Att	0.760±0.019	0.743±0.021	0.833±0.006
Anomaly + Att + SIC	<b>0.787±0.015</b>	<b>0.770±0.016</b>	<b>0.854±0.008</b>

of the University Medical Center Utrecht, the Netherlands, under reference code 15/426M and by the Ethical Committee of Clinical Investigations of Hospital Clinic, Spain (IDIBAPS) under reference code 2013/8436. Further blood samples of SCD patients were produced for MemSID (NCT02615847) clinical trial. The study protocol for it was approved by the Ethics committee of Canton Zurich (KEK-ZH 2015-0297) and the regulatory authority. Our dataset contains 3630 microscopic images taken from 71 patients/healthy individuals at different times and under variant treatments. The distribution of data in different classes is as follows: Sickle Cell Disease (SCD, 13 patients, 170 image sets), Thalassemia (Thal, 3 patients, 25 image sets), Hereditary Xerocytosis (Xero, 9 patients, 56 image sets), and Hereditary Spherocytosis (HS, 13 patients, 89 image sets). Also, we have a healthy control group (33 individuals, 181 image sets), used as negative bags.

**Training.** For training we considered 3-fold cross-validation and 100 epochs. We have two training sets: i) one set containing only control samples to estimate GMM, and ii) an other set containing a mixture of samples from all classes to train our network. We considered one GMM component with full covariance and iterated an EM algorithm up to 100 times. Mixed data are fed to the MIL classifier and every 5 epoch, control set is fed to the model to calibrate GMM parameters with updates. For optimization, we use the Adam optimizer [15] with the learning rate of  $5 \times 10^{-5}$  and weight decay of  $10^5$ . We chose the dynamic SIC loss coefficient  $\beta(e)$  as  $0.95^e$ .

### 3.1 Classification

Our metrics for classification evaluation are average accuracy, F1 score, and area under the precision recall curve (AUC). Table 1 shows our results (Anomaly + Att + SIC) in comparison with other strategies proposed by Ilse et al. [10] (Att) and Sadafi et al. [16] (Att + SIC). In addition, as an ablation study, we show the performance of our proposed anomaly scoring without SIC loss (Anomaly + Att) and attention mechanism (Anomaly). The class-wise performance of our proposed method compared to other methods is shown in Fig. 2.

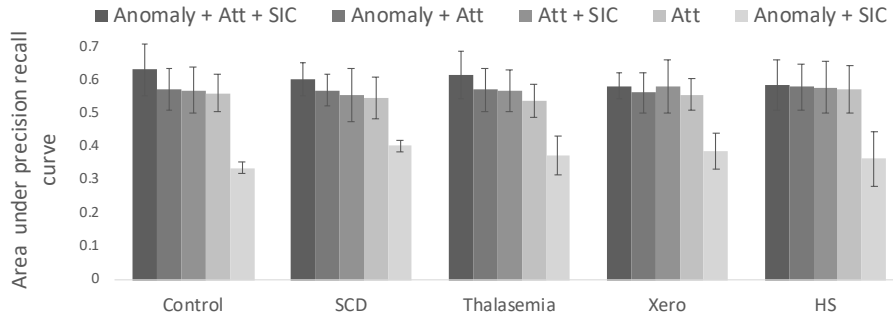


Fig. 2: Average and standard deviation of the class-wise area under precision recall curve in five runs. In all classes, our novel method outperforms others.

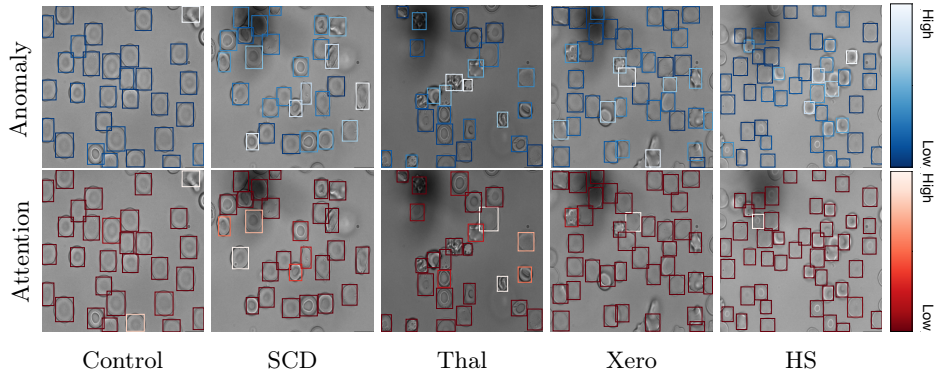


Fig. 3: Interpretation of bag classification at the instance level based on anomaly (top) and attention (bottom) scores. Compared with attention mechanism, disorder-relevant cells are more accurately scored by the anomaly mechanism.

### 3.2 Explainability

Our method’s anomaly scoring mechanism is interpretable at the instance level. In Fig. 3, for each class, we visualized a sample image, in which anomaly and attention scores are depicted by the color of the cell’s bounding box. The anomaly mechanism can distinguish class-related cells better than the attention mechanism, which is particularly striking for the SCD case, where irregular elliptoid cells are missed by the attention mechanism (Fig. 3). In Fig. 4 we show the distribution of scores assigned to cells in the test data. The frequency of both anomaly and attention scores are focused around zero, which is compatible with a majority of healthy cells (see also Fig. 4). On the other hand, for HHA, a small distribution of high scores notifies the anomalous cells. These cells show HHA properties.

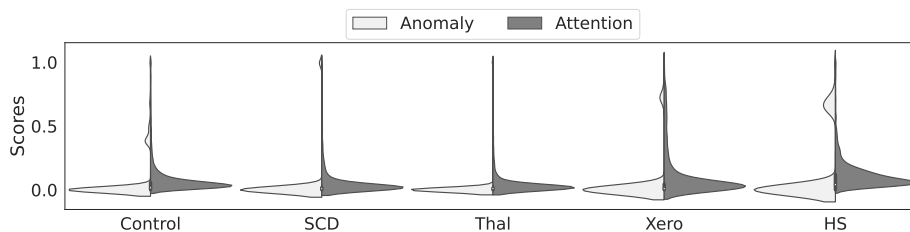


Fig. 4: Distribution of anomaly scores compared to attention scores in every class. Our anomaly scoring mechanism can distinguish a higher fraction of disorder-relevant cells.

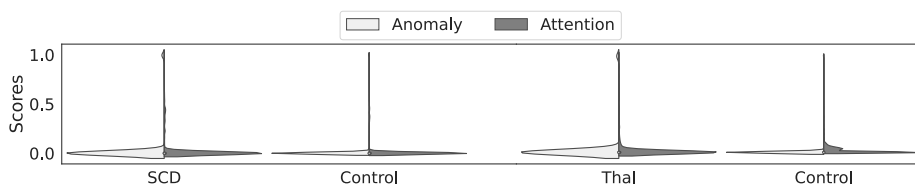


Fig. 5: Distribution of anomaly scores compared to attention scores for SCD and Thal classes when their samples were absent during the training. Our method still can assign high anomaly scores to abnormal cells.

### 3.3 Anomaly recognition

When our model estimates the distribution of control cells, high anomaly scores should be able to identify anomalous cells, whether the training set contains them or not. This property of our method is useful for detecting anomalies in rare or unseen classes during training. To examine our method in this context, we trained the model with the two HHA classes SCD and Thalassemia, separately. Then, we tested the model with unseen class samples and measured their anomaly and attention scores. Fig. 5 shows the results, where the small distribution of anomalous cells is clearly indicating anomaly awareness of the model. For both experiments, the distribution of scores in the control class is also shown.

### 3.4 CO<sub>2</sub> Emission Related to Experiments

Experiments were conducted using our in-house infrastructure with a carbon efficiency of 0.432 kgCO<sub>2</sub>eq/kWh. A cumulative 15 hours of computation was performed on the Tesla V100-SXM2-32GB (TDP of 300W) hardware. Total emissions are estimated to be 1.94 kg CO<sub>2</sub>eq. Estimations were conducted using the MachineLearning Impact calculator presented in [11].

## 4 Conclusion

We introduce anomaly-aware MIL, a simple method for enhancing classification of hereditary hemolytic anemias. Evaluations show that our method outperforms



other MIL classifiers and provides an instance-level explanation for bag-level classification results. Moreover, our novel scoring mechanism identifies anomalies in rare disease, even if they have not been seen in training sets. An interesting future work would be to upgrade the anomaly scoring to deep-learning-based out-of-distribution detection method. Another interesting future work would be uncertainty estimation on anomalous instances, which might lead to a better understanding of models coverage in representation space.

**Acknowledgements** The Helmholtz Association supports the present contribution under the joint research school “Munich School for Data Science - MUDS”. C.M. has received funding from the European Research Council (ERC) under the European Union’s Horizon 2020 research and innovation programme (Grant agreement No. 866411). CoMMiTMenT study was funded by the the European Seventh Framework Program under grant agreement number 602121 (CoMMiT-MenT) and from the European Union’s Horizon 2020 Research and Innovation Programme. MemSID (NCT02615847) clinical trial was funded by the Foundation for Clinical Research Hematology for supporting the clinical trail at the Division of Hematology, University Hospital Zurich, and, partially, by the following foundations: Baugarten Zürich Genossenschaft und Stiftung, the Ernst Goehner Stiftung, the René und Susanna Braginsky Stiftung, the Stiftung Symphysis and the Botnar Foundation.” Further funding for analysis of the obtained data was obtained European Union’s Horizon 2020 Research and Innovation Programme under grant agreement number 675115-RELEVANCE-H2020-MSCA-ITN-2015/H2020-MSCA-ITN-2015.

## References

1. Bessis, M.: *Corpuscles: Atlas of Red Blood Cell Shape*. Springer Science & Business Media (2012)
2. Bi, Q., Yu, S., Ji, W., Bian, C., Gong, L., Liu, H., Ma, K., Zheng, Y.: Local-global dual perception based deep multiple instance learning for retinal disease classification. In: *International Conference on Medical Image Computing and Computer-Assisted Intervention*. pp. 55–64. Springer (2021)
3. Campanella, G., Hanna, M.G., Geneslaw, L., Mirafior, A., Werneck Krauss Silva, V., Busam, K.J., Brogi, E., Reuter, V.E., Klimstra, D.S., Fuchs, T.J.: Clinical-grade computational pathology using weakly supervised deep learning on whole slide images. *Nature medicine* **25**(8), 1301–1309 (2019)
4. Fermo, E., Vercellati, C., Bianchi, P.: Screening tools for hereditary hemolytic anemia: new concepts and strategies. *Expert review of hematology* **14**(3), 281–292 (2021)
5. Fujita, S., Han, X.H.: Cell detection and segmentation in microscopy images with improved mask r-cnn. In: *Proceedings of the Asian Conference on Computer Vision* (2020)
6. He, K., Gkioxari, G., Dollár, P., Girshick, R.: Mask r-cnn. In: *Proceedings of the IEEE international conference on computer vision*. pp. 2961–2969 (2017)

7. He, K., Zhang, X., Ren, S., Sun, J.: Deep residual learning for image recognition. In: Proceedings of the IEEE conference on computer vision and pattern recognition. pp. 770–778 (2016)
8. Huisjes, R., van Solinge, W., Levin, M., van Wijk, R., Riedl, J.: Digital microscopy as a screening tool for the diagnosis of hereditary hemolytic anemia. *International Journal of Laboratory Hematology* **40**(2), 159–168 (2018)
9. Huisjes, R., Makhro, A., Llaudet-Planas, E., Hertz, L., Petkova-Kirova, P., Verhagen, L.P., Pignatelli, S., Rab, M.A., Schiffelers, R.M., Seiler, E., et al.: Density, heterogeneity and deformability of red cells as markers of clinical severity in hereditary spherocytosis. *haematologica* **105**(2), 338 (2020)
10. Ilse, M., Tomczak, J., Welling, M.: Attention-based deep multiple instance learning. In: International conference on machine learning. pp. 2127–2136. PMLR (2018)
11. Lacoste, A., Luccioni, A., Schmidt, V., Dandres, T.: Quantifying the carbon emissions of machine learning. arXiv preprint arXiv:1910.09700 (2019)
12. Li, S., Liu, Y., Sui, X., Chen, C., Tjio, G., Ting, D.S.W., Goh, R.S.M.: Multi-instance multi-scale cnn for medical image classification. In: International Conference on Medical Image Computing and Computer-Assisted Intervention. pp. 531–539. Springer (2019)
13. Lu, M.Y., Chen, T.Y., Williamson, D.F., Zhao, M., Shady, M., Lipkova, J., Mahmood, F.: Ai-based pathology predicts origins for cancers of unknown primary. *Nature* **594**(7861), 106–110 (2021)
14. Lu, M.Y., Williamson, D.F., Chen, T.Y., Chen, R.J., Barbieri, M., Mahmood, F.: Data-efficient and weakly supervised computational pathology on whole-slide images. *Nature biomedical engineering* **5**(6), 555–570 (2021)
15. Reddi, S.J., Kale, S., Kumar, S.: On the convergence of adam and beyond. arXiv preprint arXiv:1904.09237 (2019)
16. Sadafi, A., Makhro, A., Bogdanova, A., Navab, N., Peng, T., Albarqouni, S., Marr, C.: Attention based multiple instance learning for classification of blood cell disorders. In: International Conference on Medical Image Computing and Computer-Assisted Intervention. pp. 246–256. Springer (2020)
17. Sadafi, A., Makhro, A., Livshits, L., Navab, N., Bogdanova, A., Albarqouni, S., Marr, C.: Sickle cell disease severity prediction from percoll gradient images using graph convolutional networks. In: Domain Adaptation and Representation Transfer, and Affordable Healthcare and AI for Resource Diverse Global Health, pp. 216–225. Springer (2021)
18. Shi, X., Xing, F., Xie, Y., Zhang, Z., Cui, L., Yang, L.: Loss-based attention for deep multiple instance learning. In: Proceedings of the AAAI Conference on Artificial Intelligence. vol. 34, pp. 5742–5749 (2020)
19. Wu, Y., Schmidt, A., Hernández-Sánchez, E., Molina, R., Katsaggelos, A.K.: Combining attention-based multiple instance learning and gaussian processes for ct hemorrhage detection. In: International Conference on Medical Image Computing and Computer-Assisted Intervention. pp. 582–591. Springer (2021)